Deduction Measurement Method and High-Accuracy Calculation Model of Leakage Flux Eddy Current Loss in Nanocrystalline Core High-Frequency Transformer

Zhanlei Liu, *Student Member, IEEE*, Lingyu Zhu, *Senior Member, IEEE*, Yongliang Dang, Cao Zhan, *Member, IEEE*, and Shengchang Ji, *Member, IEEE*

***Abstract*—The normal leakage flux induces strong eddy currents on the surface of nanocrystalline core, producing significant leakage flux eddy current loss (LFECL). Since LFECL is proportional to the square of current, LFECL resistance (LFECLR) is proposed in this article to characterize the LFECL. A deduction measurement method for LFECLR in nanocrystalline core is proposed. The LFECLR can be obtained by deduction of winding ac resistance and core loss resistance from total ac resistance under short-circuit conditions. The winding ac resistance can be measured on a ferrite core HFT with identical core and winding sizes, and the core loss resistance can be calculated by finite element (FE) simulation. A homogenization FE model considering air gap and frequency-dependent permeability is proposed for accurate calculation of LFECLR. The mean errors of the proposed model for two HFT prototypes are reduced from 55.9% and 12.5% to 2.56% and 7.2%. In addition, the impacts of air gap length, permeability, and frequency on LFECLR are investigated. Simulation results show that LFECLR decreases with permeability and increases with frequency. For the HFT with concentric windings, LFECLR first increases and then decreases with air gap length. For the HFT with separated windings, LFECLR decreases with air gap length.**

***Index Terms*—Deduction measurement method, eddy current loss, high-frequency transformer (HFT), homogenization finite element (FE) model, leakage flux, nanocrystalline core.**

I. Introduction

As a key component in isolated dc–dc converters, high-frequency transformer (HFT) obtains wide applications in electric vehicle charging station [1], [2], railway transportation [3], [4], dc distribution grid [5], [6], energy storage station [1], [5], etc. Taking advantage of high saturated flux density and low power loss density, nanocrystalline core is preferred in high-frequency (10–50 kHz) and high-power (>20 kW) occasions [7].

Accurate estimation of core loss is nontrivial and has attracted a lot of attention. Empirical equations [8], [9], [10], [11], [12], [13], [14] and loss separation formulas [15], [16], [17], [18], [19], [20] have been proposed to predict the core loss under non-sinusoidal excitations. The empirical equations are applied to the core loss calculation in the optimal design of HFT prototypes in [21], [22], [23]. However, these approaches only consider the core loss caused by the main flux density. Finite element (FE) model and equivalent circuit model [24], [25] are developed to calculate eddy current loss in steel laminations with edge burrs. However, these models only calculate the eddy current loss in the lamination section. In nanocrystalline core, as illustrated in Fig. 1, the normal leakage flux can produce large eddy currents in the ribbon plane, increasing the total core loss. In high-leakage-inductance or magnetic-integrated HFTs, the leakage magnetic field in the core window is large and the leakage flux eddy current loss (LFECL) becomes more significant. In addition, the leakage flux eddy currents are concentrated on the surface of nanocrystalline core [26], [27], [28], resulting in local hotspots and insulation risks. Therefore, accurate estimation of LFECL is crucial.

The thermal image approach provides an initial observation of LFECL under short-circuit conditions through local hotspots caused by local eddy currents [26], [27], [28]. However, the value of LFECL cannot be measured. Impedance analyzer can be used to measure the ac resistance of transformer under

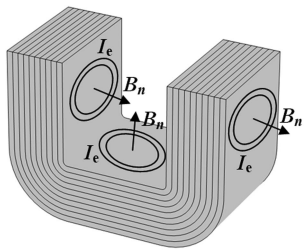

Fig. 1. Schematic of leakage flux eddy currents in nanocrystalline core.

Received 25 July 2024; revised 17 October 2024; accepted 30 November 2024. Date of publication 9 December 2024; date of current version 28 January 2025. This work was supported by State Key Laboratory of HVDC under Grant SKLHVDC-2023-KF-10. Recommended for publication by Associate Editor D. Vinnikov. *(Corresponding author: Lingyu Zhu.)*

Zhanlei Liu, Lingyu Zhu, Yongliang Dang, and Shengchang Ji are with the State Key Laboratory of Electrical Insulation and Power Equipment, Xi'an Jiaotong University, Xi'an 710049, China (e-mail: lzl0283@stu.xjtu.edu.cn; zhuly1026@xjtu.edu.cn; dyl877759724@stu.xjtu.edu.cn; jsc@xjtu.edu.cn).

Cao Zhan is with the Bradley Department of Electrical and Computer Engineering, Center for Power Electronics Systems, Virginia Tech, Blacksburg, VA 24061 USA (e-mail: caozhan@vt.edu).

Color versions of one or more figures in this article are available at https://doi.org/10.1109/TPEL.2024.3512856.

Digital Object Identifier 10.1109/TPEL.2024.3512856

short-circuit condition. The measured ac resistance includes both core loss equivalent resistance and winding resistance. A method is proposed to separate core loss equivalent resistance and winding resistance in [29]. However, the LFECL resistance (LFECLR) cannot be separated from total core loss equivalent resistance for nanocrystalline core. Homogenization FE model for nanocrystalline core is established to calculate the leakage flux density and eddy current density distributions. The LFECL is calculated by the volume integration of eddy current loss density over the core region [30], [31], [32], [33]. However, these simulations are implemented under sinusoidal excitations of fundamental frequency. LFECL at higher frequencies has not been investigated. In addition, the air gap is not considered in the FE simulations and the impact of air gap length on the eddy current loss has not been fully understood.

To address the aforementioned issues, this article proposes a deduction measurement method and high-accuracy calculation model for the LFECLR in nanocrystalline core. The main contributions of this article are as follows.

1) A deduction measurement method for the LFECLR under sinusoidal excitation is proposed.
2) A high-accuracy calculation model for the LFECLR in nanocrystalline core is proposed, in which air gap and frequency-dependent permeability are identified as significant parameters and should be considered.
3) The impacts of air gap length, permeability, and frequency on the LFECLR are analyzed. A magnetic circuit model is established to explain the variations of LFECLR with air gap length and permeability. FE simulations are implemented to analyze the parameter sensitivity.

The rest of this article is organized as follows. In Section II, the homogenization FE model is introduced and the leakage flux eddy current distributions in nanocrystalline core for two HFT prototypes are analyzed. In Section III, the principle and results of the proposed deduction measurement method are presented. In Section IV, the proposed high-accuracy calculation model for LFECLR is introduced. The calculation results with and without considering air gap and frequency-dependent permeability are compared with experimental results. In Section V, the impacts of air gap length and frequency-dependent permeability on LFECLR are studied. Theoretical analysis based on magnetic circuit theory and sensitivity analysis based on FE simulation are provided. Finally, Section VI concludes this article.

II. Analysis of Leakage Flux Eddy Current by Homogenization FE Model

In nanocrystalline core, the normal leakage flux induces eddy currents in surface ribbons, which is referred to as leakage flux eddy current in this article. Two nanocrystalline UU-core HFTs with concentric windings and separated windings in a single core leg, as shown in Fig. 2, are taken as cases for investigation in this article. The dimensions of nanocrystalline core and windings of the two HFT prototypes are shown in Fig. 3. The turn ratios of these two HFTs are 9:9 and 10:10, respectively. The respective leakage inductances of these two HFTs at 20 kHz are 5.74 μH and 19.4 μH. Homogenization FE model is adopted to calculate the leakage flux eddy current distributions in the nanocrystalline core.

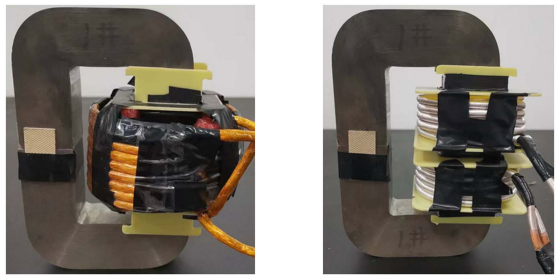

Fig. 2. Nanocrystalline UU-core HFTs with (a) concentric windings and (b) separated windings in one core leg.

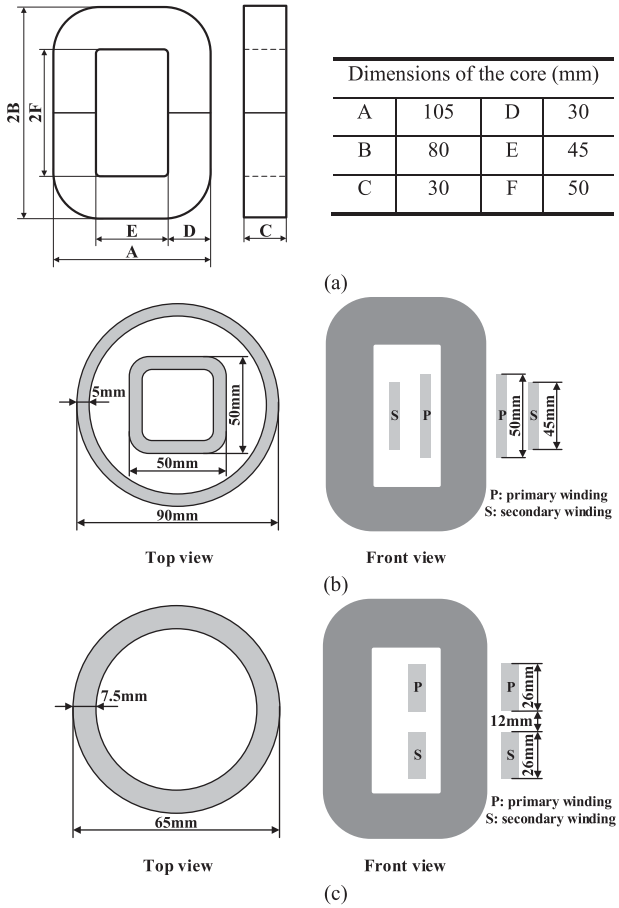

Fig. 3. Dimensions of (a) nanocrystalline core, (b) windings of concentric winding HFT, and (c) windings of separated winding HFT in this paper.

A. Homogenization FE Model

The nanocrystalline core is produced by the rolling of ribbons with epoxy resin filled in the interlayers to insulate the eddy currents. Since nanocrystalline ribbon is very thin and fine meshing of individual ribbons is not feasible, homogenization approach with anisotropic conductivity and permeability [34], [35], [36], [37] is adopted to model the nanocrystalline core

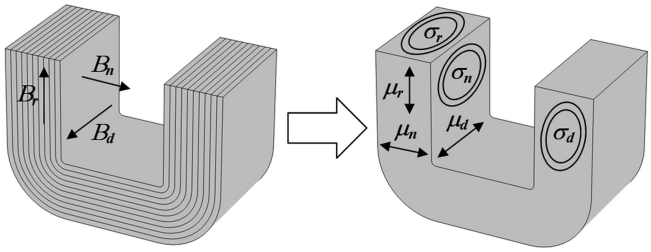

Fig. 4. Homogenization model of nanocrystalline core.

TABLE I
PARAMETERS IN THE HOMOGENIZATION FE MODEL

F	μ_m	σ_m(S/m)	μ_r and μ	μ_n	σ_r and σ_d(S/m)	σ_n(S/m)
0.78	33580	8.7×10^5	26192.6	4.545	6.78×10^5	0.4955

as illustrated in Fig. 4. The selected U-shape nanocrystalline core in this article is made by Fe-based nanocrystalline alloy from Advanced Technology & Materials Co., Ltd in China. The specific composition is $Fe_{73.5}Cu_1Nb_3Si_{15.5}B_7$. The width of the nanocrystalline core is 30 mm. The thickness of the nanocrystalline ribbon is 20 μm and the filling factor is about 0.78. At a frequency of 20 kHz and temperature of 25 °C, the parameters in the homogenization FE model are listed in Table I, where μ_r, μ_d, and μ_n are the equivalent permeabilities in the rolling direction, thick direction, and normal direction, σ_r, σ_d, and σ_n are the equivalent conductivities in the rolling direction, thick direction, and normal direction, F is filling factor, μ_0 is the vacuum permeability, μ_m is the permeability of the ribbons, σ_m is the conductivity of the ribbons.

Since a rectangular nanocrystalline core is formed by putting together two U-cores, a small air gap in the split joint is produced. To calculate the average length of air gap, the magnetizing inductance of the transformer is measured by an impedance analyzer, being $L_m = 405$ μH. According to (1), the equivalent relative permeability of nanocrystalline core is $\mu_r = 1607$. By magnetic reluctance (2), the length of air gap is 0.1 mm

$$\mu = \mu_0\mu_r = L_m \frac{l}{N^2 A_e} \tag{1}$$

$$\frac{l_{\text{nano}}}{\mu_{\text{nano}} F S} + \frac{l_{\text{air}}}{\mu_0 S} = \frac{l}{\mu_r S} \tag{2}$$

where N is the number of turns, l is the length of magnetic circuit, A_e is the area of cross-section, l_{nano} and l_{air} are the magnetic circuit length of nanocrystalline and air gap, and μ_{nano} is the permeability of nanocrystalline ribbon.

B. Simulation Results

The frequency-domain solver in COMSOL Multiphysics software is used to calculate the leakage flux density and leakage flux eddy current density distributions in the core. Figs. 5(a) and 6(a) show the nonuniform leakage flux density amplitude distributions in the nanocrystalline core. Due to the low permeability in the normal direction to the ribbons and the demagnetization effect of leakage flux eddy current in the ribbon planes, most of the magnetic flux is concentrated in a very thin layer on the surface of the core near the winding endings. The flux density inside the core is very small.

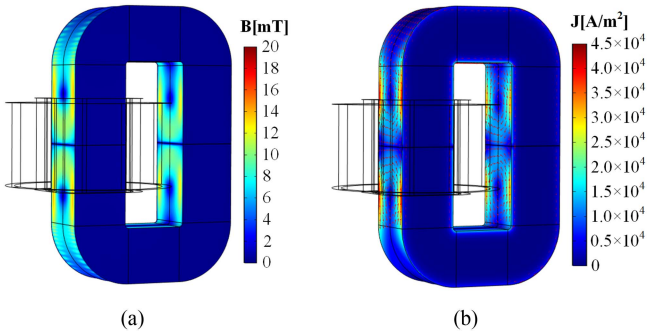

Fig. 5. (a) Flux density amplitude and (b) leakage flux eddy current density amplitude distributions in nanocrystalline core HFT with concentric windings ($f = 20$ kHz, $I_p = 1$ A).

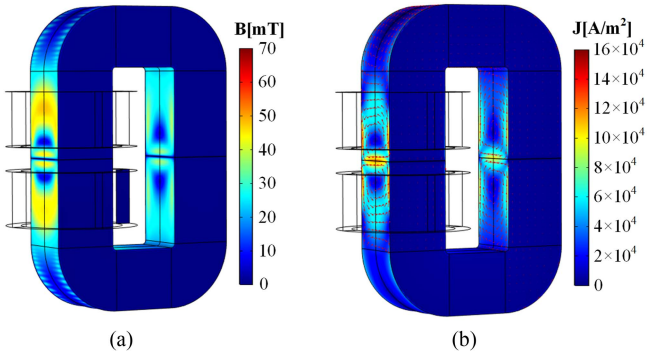

Fig. 6. (a) Flux density amplitude and (b) leakage flux eddy current density amplitude distributions in nanocrystalline core HFT with separated windings ($f = 20$ kHz, $I_p = 1$ A).

Figs. 5(b) and 6(b) show the leakage flux eddy current density amplitude distributions in the nanocrystalline core. Due to the normal leakage flux on the core surface and the high conductivity in the ribbon plane, significant circulating eddy currents are localized in a thin layer on the core surface near the winding endings. These eddy currents contribute to the total nanocrystalline core loss.

A comparison of Figs. 5 and 6 shows that the leakage flux density and leakage flux eddy current density in the HFT with separated windings are larger than the HFT with concentric windings. The reason is that the leakage magnetic field and leakage inductance in the HFT with separated windings is higher. Therefore, the LFECL in the HFT with separated windings will be larger.

Fig. 7 shows the local leakage flux eddy current density amplitude distributions of the HFT with concentric winding. As shown in Fig. 7(a), the thickness of surface eddy current layer in the gapped core is greater than the nongapped core. As shown in Fig. 7(b), the thickness of surface eddy current layer in the gapped core decreases with permeability. Thus, the LFECL will differ with air gap and permeability.

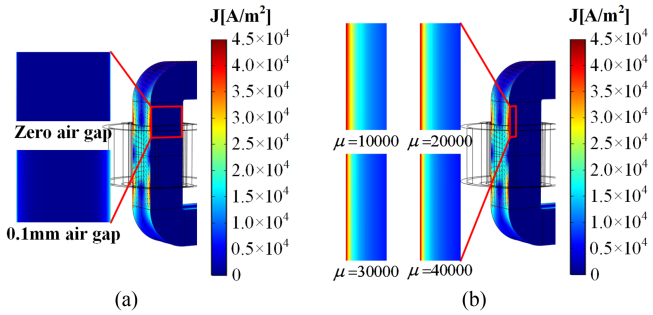

Fig. 7. Comparison of leakage flux eddy current density amplitude distributions (a) with and without air gap and (b) with different permeability in nanocrystalline core HFT with concentric windings ($f = 20$ kHz, $I_p = 1$ A).

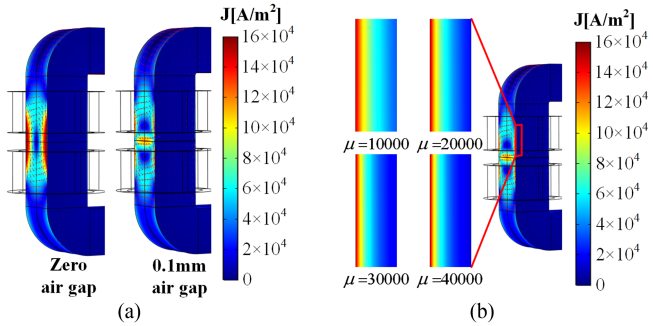

Fig. 8. Comparison of leakage flux eddy current density amplitude distributions (a) with and without air gap and (b) with different permeability in nanocrystalline core HFT with separated windings ($f = 20$ kHz, $I_p = 1$ A).

Fig. 8 shows the local leakage flux eddy current density amplitude distributions of the HFT with separated winding. As shown in Fig. 8(a), the air gap will cut off the leakage flux eddy current path, reducing the leakage flux eddy current density. As shown in Fig. 8(b), the thickness of surface eddy current layer in the gapped core decreases with permeability. Thus, the LFECL will differ with air gap and permeability.

III. Deduction Method for LFECLR Measurement

When secondary winding of a transformer is short-circuited and primary winding is excited, according to Ampere's loop law, the magnetic field intensity H is proportional to the current of primary winding I

$$H \propto I. \tag{3}$$

From the electromagnetic field constitutive equation, in the linear magnetization region, magnetic flux density B is proportional to magnetic field intensity H

$$B = \mu H. \tag{4}$$

Adopting Faraday's electromagnetic induction law, the induced electromotive force is proportional to dB/dt. Therefore, the induced eddy current is proportional to dB/dt, and LFECL P_{leakage} is proportional to the square of dB/dt

$$P_{\text{leakage}} \propto (\mathrm{d}B/\mathrm{d}t)^2. \tag{5}$$

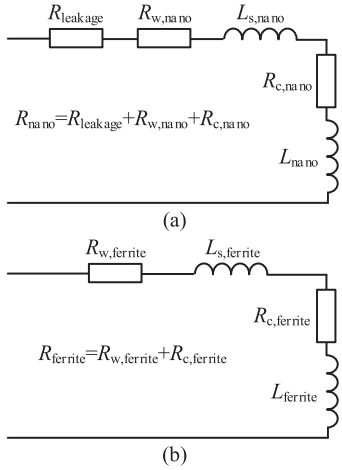

Fig. 9. Equivalent circuits of (a) nanocrystalline core HFT and (b) ferrite core HFT under short-circuit condition.

Combining (3)–(5), LFECL is proportional to the square of current. Therefore, LFECLR is defined in this article to characterize the LFECL. The LFECLR R_{leakage} can be expressed as

$$R_{\text{leakage}} = P_{\text{leakage}}/I^2. \tag{6}$$

Direct measurement of LFECL is nontrivial since it is accompanied by winding loss and magnetic loss. In this section, a deduction method is proposed for LFECLR measurement.

A. Principle of the Deduction Method

The total ac resistance of a nanocrystalline core HFT under short-circuit condition R_{nano} includes the winding ac resistance $R_{w,\text{nano}}$, core loss equivalent resistance $R_{c,\text{nano}}$, and LFECLR R_{leakage} [29], as shown in Fig. 9(a). Therefore, R_{leakage} can be expressed as

$$R_{\text{leakage}} = R_{\text{nano}} - R_{w,\text{nano}} - R_{c,\text{nano}}. \tag{7}$$

The total ac resistance of an HFT under short-circuit conditions can be measured by an impedance analyzer.

Affected by the skin effect and proximity effect of winding currents, accurate calculation of winding ac resistance at high frequency is not feasible. To obtain the precise value of winding ac resistance, an equivalent measurement method is proposed. A ferrite core HFT with identical core and winding sizes is made. The winding ac resistance of nanocrystalline core HFT is regarded as equal to the ac resistance of ferrite core HFT. The winding ac resistance equality is proved in the following.

Due to the low conductivity of ferrite core, the ac resistance of a ferrite core HFT under short-circuit condition R_{ferrite} includes only winding ac resistance $R_{w,\text{ferrite}}$ and core loss equivalent resistance $R_{c,\text{ferrite}}$ [29], as shown in Fig. 9(b). Since the permeability and conductivity of the ferrite core are isotropy, the leakage flux density distribution in the ferrite core is uniform. The ferrite core loss is small and negligible compared with the

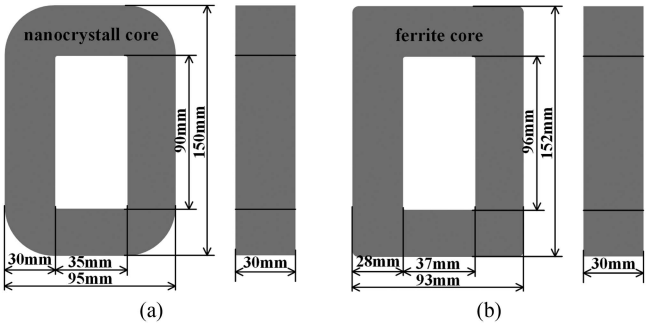

Fig. 10. Size of magnetic cores. (a) Nanocrystalline core. (b) Ferrite core.

winding ac loss. Therefore, R_{ferrite} is approximately equal to $R_{w,\text{ferrite}}$

$$R_{\text{ferrite}} = R_{w,\text{ferrite}} + R_{c,\text{ferrite}} \approx R_{w,\text{ferrite}}. \tag{8}$$

A standard ferrite core with a similar size to the nanocrystalline core utilized in Fig. 2 is selected. The ferrite core material is 3C90 from FERROXCUBE. The dc resistivity of the ferrite core at 25 °C is 5 Ωm. Slight differences in size exist between the two cores as shown in Fig. 10. Since the core sizes of the two transformers are similar, the leakage magnetic field distributions in the core window as well as the winding ac resistances will be similar. To avoid the measurement error caused by the differences in windings between two transformers, the same winding is recommended in the ac resistance measurements. In addition, litz wire is preferred for its low ac resistance at high frequency. The conduction resistance is dominant in the total ac resistance of litz wire at low frequency, which is equal for the two transformers. The induction resistance is dominant in the total ac resistance of litz wire at high frequency, which is proportional to the integration of the square of the magnetic field strength H in the winding region [38]. A FE simulation model is established, where the windings are modeled by rectangular sections with uniform current density, to investigate the leakage magnetic field distribution in the winding region. The leakage magnetic field simulation results of the two HFT prototypes are demonstrated in Fig. 11. The integration of the square of H over the winding region V is defined as Int_H2 in this article, which can be expressed as

$$\text{Int\_H2} = \int_V H^2 \mathrm{d}V. \tag{9}$$

The deviations of calculated Int_H2 between ferrite core HFT and nanocrystalline core HFT are shown in Fig. 12. Within 10–300 kHz, the maximum deviations of Int_H2 between ferrite core HFT and nanocrystalline core HFT are within 3.5% for the two HFT prototypes. Therefore, the differences in winding ac resistances between ferrite core HFT and nanocrystalline core HFT for the two HFT prototypes are within 3.5%. $R_{w,\text{nano}}$ is approximately equal to $R_{w,\text{ferrite}}$

$$R_{w,\text{nano}} \approx R_{w,\text{ferrite}}. \tag{10}$$

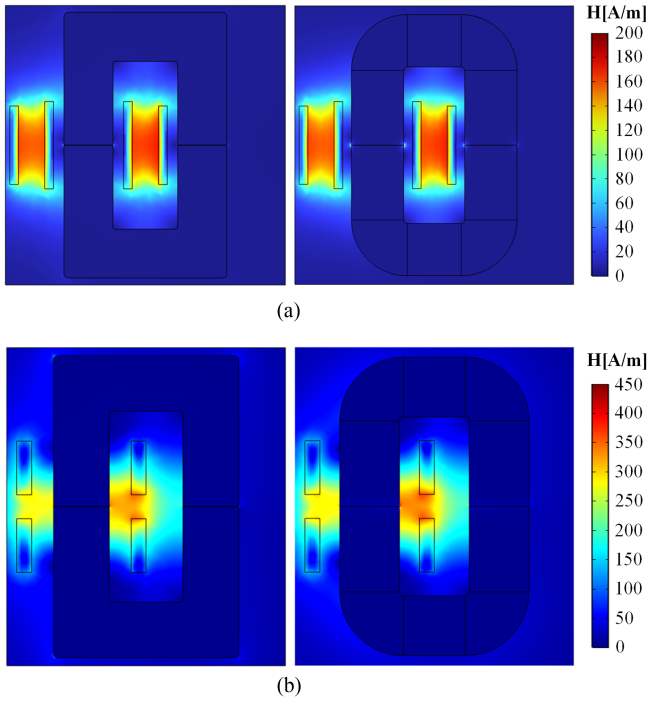

Fig. 11. Leakage magnetic field simulation results of ferrite and nanocrystalline core transformers with (a) concentric windings and (b) separated windings.

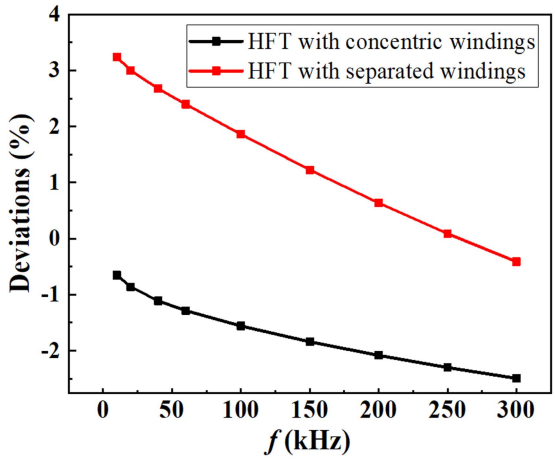

Fig. 12. Deviations of Int_H2 between ferrite core HFT and nanocrystalline core HFT.

The leakage flux density distributions in nanocrystalline core calculated by the homogenization FE model are quite nonuniform as shown in Figs. 5(a) and 6(a). The leakage flux core loss density is estimated by the Steinmetz equation (SE) [8], [39] and the total leakage flux core loss is calculated by the integration of core loss density over the core region. The leakage flux core loss equivalent resistance is estimated by

$$R_c = \frac{1}{I^2} \int_V k f^{\alpha} B_m^{\beta} \cdot \mathrm{d}V \tag{11}$$

where k, α, and β are Steinmetz coefficients. Since β is close to 2, R_c varies slightly with B_m. To accurately calculate R_c and

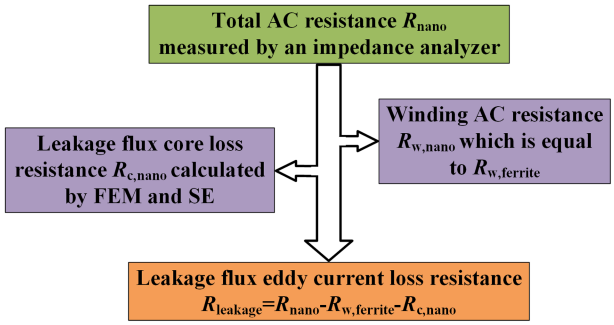

Fig. 13. Flowchart of the proposed deduction measurement method of leakage flux eddy current loss.

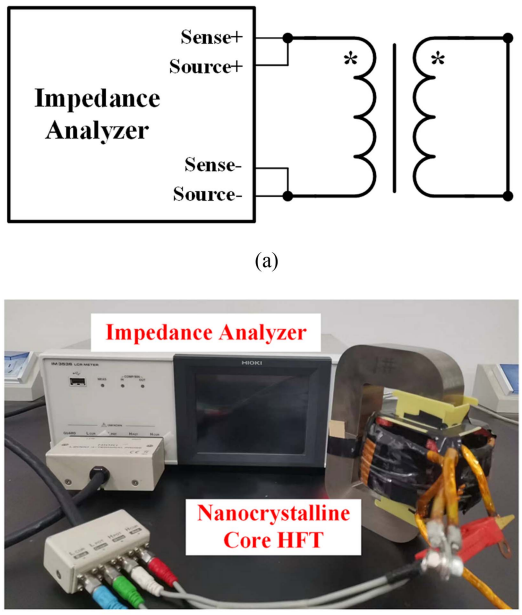

Fig. 14. AC resistance test platform of HFT by impedance analyzer. (a) Schematic diagram. (b) Experimental platform.

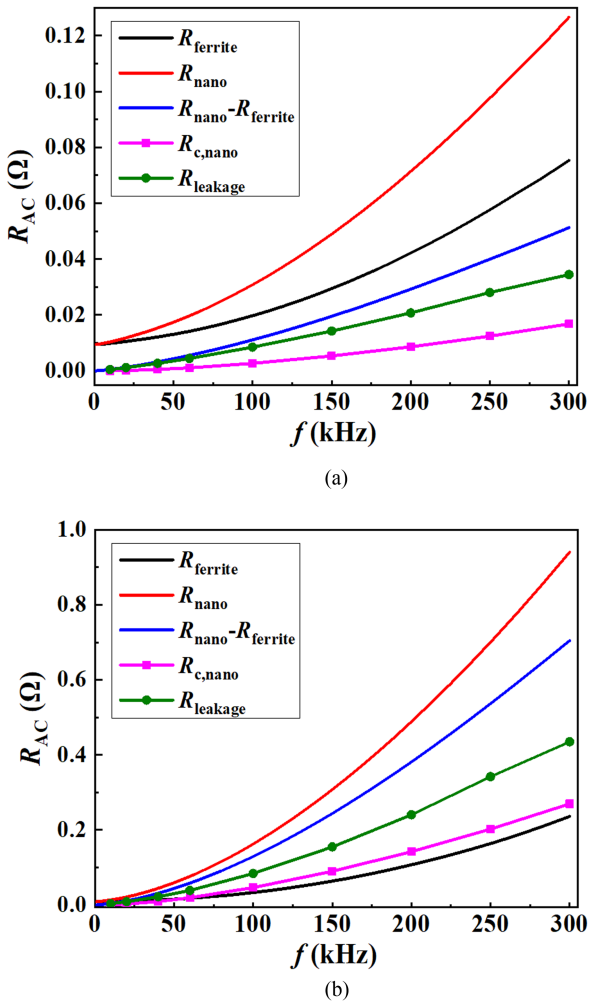

Fig. 15. AC resistances and LFECLR of (a) HFTs with concentric windings and (b) HFTs with separated windings.

R_{leakage}, the excitation condition in FE simulation is set to be identical to the measurement condition of impedance analyzer. In this way, the flux density in FE simulation will be identical to the measurement condition, and the calculated R_c will be the same as R_c in measured ac resistance.

The flowchart of the proposed deduction measurement method is shown in Fig. 13. Combining (7)–(8) and (10)–(11), the LFECLR can be expressed as

$$R_{\text{leakage}} = R_{\text{nano}} - R_{\text{ferrite}} - R_{c,\text{nano}}. \tag{12}$$

B. Measurement Results

The ac resistance test setup for HFT under short-circuit conditions is shown in Fig. 14. The impedance analyzer is IM3536 from HIOKI E.E. CORPORATION. The test frequency ranges from 10 to 300 kHz. Fig. 15 shows the measurement results, where R_{ferrite} and R_{nano} represent the total ac resistance of ferrite core HFT and nanocrystalline core HFT measured by an impedance analyzer. Due to the significant LFECL and core loss caused by the leakage flux, the ac resistance of nanocrystalline core transformer is higher than the ferrite core transformer. Since R_{ferrite} is approximately equal to $R_{w,\text{ferrite}}$, R_{nano}-R_{ferrite} includes the core loss equivalent resistance $R_{c,\text{nano}}$ and LFECLR R_{leakage} of nanocrystalline core HFT. After calculating $R_{c,\text{nano}}$, R_{leakage} can be obtained by subtraction of $R_{c,\text{nano}}$ from R_{nano}–R_{ferrite}. The ratio of LFECLR to the winding ac resistance are 12.3% and 56.4% respectively at 20 kHz and 100 kHz for the transformer with concentric winding, and are 110.5% and 390.2% respectively at 20 kHz and 100 kHz for the transformer with separated winding. The nanocrystalline core loss caused by the leakage flux is significant and non-negligible, especially at high frequencies. The ratio of leakage flux core loss to the winding ac resistance are 1.4% and 13.5% respectively at 20 kHz and 100 kHz for the transformer with concentric winding, and are 25% and 138.6% respectively at 20 kHz and 100 kHz for the transformer with separated winding. In addition, the core loss and LFECL in the transformer with separated windings are greater than the transformer with concentric windings.

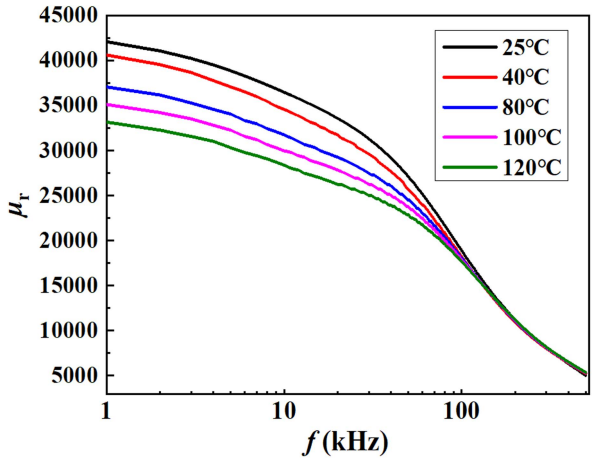

Fig. 16. Relative permeability of nanocrystalline core with frequency and temperature.

IV. Calculation Model of LFECLR Considering Air Gap and Frequency-Dependent Permeability

As demonstrated in Figs. 7 and 8, air gap and permeability can significantly change the leakage flux eddy current distribution in nanocrystalline core. Thus, to accurately calculate the LFECLR, air gap, and frequency-dependent permeability should be taken into consideration. A homogenization FE model considering air gap and frequency-dependent permeability is proposed in this section for accurate calculation of LFECLR.

A. Calculation Model

At high frequencies, the skin effect of eddy current becomes significant and the homogenization method cannot accurately calculate the eddy current density distribution in the core section. Therefore, the conductivity of the nanocrystalline ribbon in the normal direction is set to zero. The eddy current in the core section is canceled and frequency-dependent permeability is utilized to characterize the demagnetization effect of eddy currents in the core section. A small toroidal core with a winding of 20 turns is utilized to measure the magnetizing inductance and the relative permeability is calculated in (1). The selected toroidal core is also made by Fe-based nanocrystalline alloy from Advanced Technology & Materials Co., Ltd in China. The specific composition is also $Fe_{73.5}Cu_1Nb_3Si_{15.5}B_7$. The inner and outer diameters of the core are 40 mm and 25 mm respectively. The width of the core is 20 mm. The thickness of the nanocrystalline ribbon is 20 μm and the filling factor is about 0.78. As illustrated in Fig. 16, the permeability of nanocrystalline core is both frequency-dependent and temperature-dependent. From 1 to 100 kHz, the relative permeability decreases with frequency and temperature. From 100 to 500 kHz, the relative permeability of nanocrystalline core decreases with frequency and remains almost constant with temperature.

The eddy current density in the nanocrystalline core is calculated by FE simulation. The LFECL in the nanocrystalline core is calculated by the integration of eddy current loss density in the core region as

$$P_{\text{leakage}} = \int_V \frac{J^2}{\sigma} \cdot \mathrm{d}V \tag{13}$$

where J is the eddy current density and σ is the conductivity. Then, the LFECLR of the nanocrystalline core is calculated in (6).

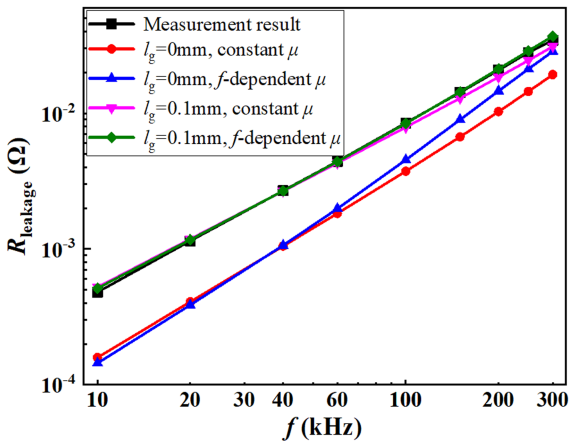

(a)

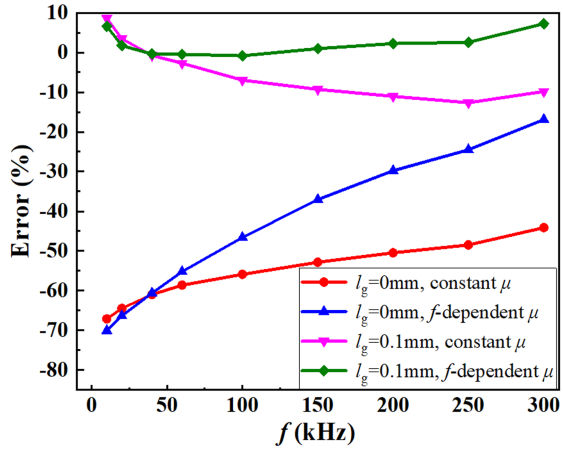

(b)

Fig. 17. (a) Comparison of calculated and measured LFECLR R_{leakage} versus frequency and (b) errors of calculated R_{leakage} versus frequency for transformer with concentric windings.

B. Calculation Results

Fig. 17(a) shows the measured and calculated LFECLR R_{leakage} for the transformer with concentric windings. The FE model considering air gap and frequency-dependent permeability can accurately calculate the LFECLR. However, the FE model without considering the air gap will greatly underestimate the eddy current loss, and FE model without considering the frequency-dependent permeability will slightly underestimate the eddy current loss at high frequency. Fig. 17(b) shows the errors of calculated R_{leakage}. The maximum error and mean error of the FE model considering air gap and frequency-dependent permeability are 7.25% and 2.56%, respectively. The maximum

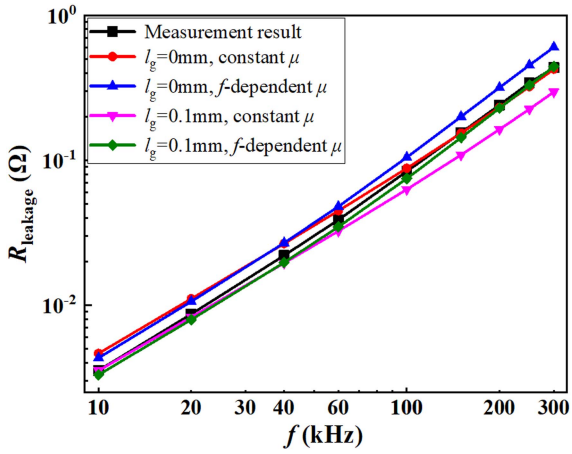

(a)

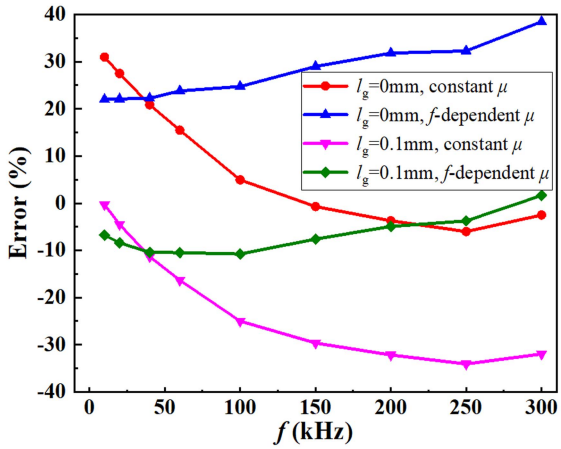

(b)

Fig. 18. (a) Comparison of calculated and measured LFECLR R_{leakage} versus frequency and (b) errors of calculated R_{leakage} versus frequency for HFT with separated windings.

errors and mean errors of the FE model with $l_g = 0$ mm and constant u, $l_g = 0$ mm and frequency-dependent u and $l_g = 0.1$ mm and constant u are 67.1% and 55.9%, 70.1% and 12.6%, and 45.2% and 7.3%, respectively. The impact of the air gap on the LFECLR is greater than the frequency-dependent permeability.

Fig. 18(a) shows the measured and calculated LFECLR R_{leakage} for the transformer with separated windings. The FE model considering air gap and frequency-dependent permeability can accurately calculate the LFECLR. However, the FE model without considering the air gap will greatly overestimate the eddy current loss, and the FE model without considering the frequency-dependent permeability will slightly underestimate the eddy current loss at high frequency. Fig. 18(b) shows the errors of calculated R_{leakage}. The maximum error and mean error of the FE model considering air gap and frequency-dependent permeability are 10.8% and 7.2% respectively. The maximum errors and mean errors of the FE model with $l_g = 0$ mm and constant u, $l_g = 0$ mm and frequency-dependent u and $l_g = 0.1$ mm and constant u are 31.0% and 12.5%, 38.5% and 27.4%, and 34.1% and 20.6%, respectively. Both the impact of the air gap and frequency-dependent permeability on the LFECLR are significant.

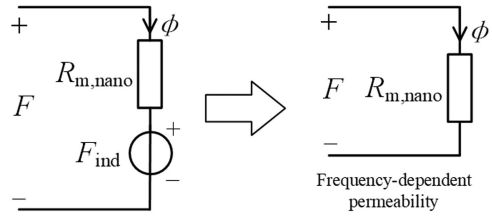

Fig. 19. Equivalent magnetic circuit of a single ribbon.

V. Impact of Air Gap Length and Frequency-Dependent Permeability on LFECLR

The leakage flux and leakage flux eddy current distributions in a nanocrystalline core are affected by the air gap length and permeability. Theoretic analysis and simulation calculation are conducted in this section to investigate the impact of air gap length and frequency-dependent permeability on the LFECLR.

A. Theoretic Analysis

The uneven leakage flux distribution in the nanocrystalline core is mainly caused by two factors. The first factor is the anisotropic permeability. Since the permeability of epoxy resin between nanocrystalline ribbons is low, the equivalent permeability of nanocrystalline core in the normal direction to the ribbon plane is extremely low. Therefore, the leakage flux is difficult to penetrate the core. The second factor is the demagnetization effect of the leakage flux eddy current. A reverse magnetic field is induced by the leakage flux eddy current, preventing the leakage flux from penetrating internal ribbons. Therefore, most of the leakage flux is concentrated on the surface of the core. The air gap and frequency-dependent permeability will change the equivalent permeability of the nanocrystalline core, and then change the leakage flux distribution and LFECL. The magnetic circuit theory can be applied to analyze the impact of air gap length and frequency-dependent permeability on the leakage flux distribution and LFECL.

The equivalent magnetic circuit of a single nanocrystalline ribbon is shown in Fig. 19, where F is the MMF, $R_{m,\text{nano}}$ is the reluctance of nanocrystalline ribbon, F_{ind} is the reverse MMF induced by the eddy currents in the ribbon section, ϕ is the magnetic flux. Magnetic flux ϕ can be calculated by $\phi = (F\text{-}F_{\text{ind}})/R_{\text{nano}}$. With the increase of frequency, F_{ind} increases and ϕ decreases. Therefore, the effective permeability decreases with frequency. The frequency-dependent permeability measured on the toroidal core as shown in Fig. 16 can account for the effect of induced reverse magnetic flux. Hence, the reverse MMF source can be removed from the magnetic circuit by applying frequency-dependent permeability.

For HFT with concentric windings, taking several ribbons as illustrated in Fig. 20(a) as an example, an equivalent magnetic circuit is established as illustrated in Fig. 20(b), where F is

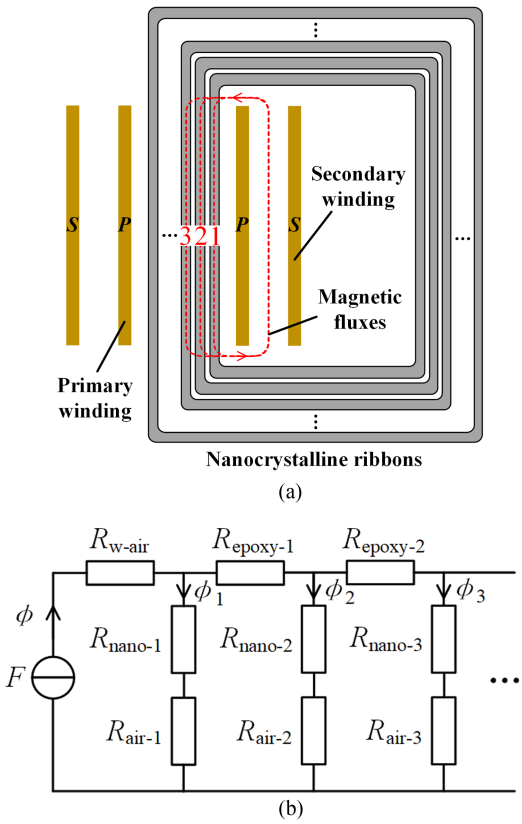

Fig. 20. Schematic diagram of leakage flux paths in the HFT with concentric windings. (a) An example of leakage flux paths in the nanocrystalline core composed of several ribbons. (b) Equivalent magnetic circuit model.

the magnetomotive force, ϕ is the magnetic flux, $R_{w\text{-air}}$ is the reluctance of air in the core window, $R_{\text{epoxy-1}}$ and $R_{\text{epoxy-2}}$ are the reluctance of the first and second layers of epoxy resin, respectively, $R_{\text{nano-1}}$, $R_{\text{nano-2}}$, and $R_{\text{nano-3}}$ are the reluctance of the first, second, and third layers of nanocrystalline ribbons, respectively, $R_{\text{air-1}}$, $R_{\text{air-2}}$, and $R_{\text{air-3}}$ are the reluctance of air gap in the first, second, and third layers of nanocrystalline ribbons, respectively. The reverse MMF sources, which model the reverse magnetic flux induced by the eddy currents in ribbon sections, are not connected in series with $R_{\text{nano},i}$ in Fig. 20(b). Instead, frequency-dependent permeability is adopted to account for the demagnetization effect of induced eddy currents in ribbon sections. Due to the low permeability of air and large air length in the core window, $R_{w\text{-air}}$ is far greater than the reluctances of ribbon, epoxy resin, and air gap. Assuming $R_{\text{air-1}} = R_{\text{air-2}} = R_{\text{air-3}} = R_{\text{air}}$, $R_{\text{nano-1}} = R_{\text{nano-2}} = R_{\text{nano-3}} = R_{\text{nano}}$, and $R_{\text{epoxy-1}} = R_{\text{epoxy-2}} = R_{\text{epoxy}}$, the magnetic flux in the third ribbon can be expressed as

$$\phi_3 = \frac{F/R_{w-\text{air}}}{\left[\left(\frac{R_{\text{epoxy}}}{R}\right)^2 + 4\frac{R_{\text{epoxy}}}{R} + 3\right] + \left[\left(\frac{R_{\text{epoxy}}}{R}\right)^2 + 3\frac{R_{\text{epoxy}}}{R} + 1\right]\frac{R}{R_{w-\text{air}}}} \tag{14}$$

where $R = R_{\text{nano}} + R_{\text{air}}$.

When the length of air gap is small, $R_{w\text{-air}}$ is far greater than the reluctances of ribbon, epoxy resin, and air gap, $R/R_{w\text{-air}}$ can be ignored and ϕ_3 is simplified as

$$\phi_3 = \frac{F/R_{w-\text{air}}}{\left(\frac{R_{\text{epoxy}}}{R}\right)^2 + 4\frac{R_{\text{epoxy}}}{R} + 3}. \tag{15}$$

With the increase of the air gap length l_g, R_{air} increases and ϕ_3 increases. Thus, the leakage magnetic flux penetrating the internal ribbon increases, leading to the increases of leakage flux eddy current in the internal ribbons and the total LFECL.

When the length of air gap is large, R_{air} is large, $R/R_{w\text{-air}}$ cannot be ignored and R_{epoxy}/R can be ignored. Thus, ϕ_3 is simplified as

$$\phi_3 = \frac{F/R_{w-\text{air}}}{3 + \frac{R}{R_{w-\text{air}}}}. \tag{16}$$

With the increase of the air gap length l_g, R_{air} increases and ϕ_3 decreases. Thus, the leakage magnetic flux penetrating the internal ribbon decreases, leading to the decrease of leakage flux eddy current in the internal ribbons and the total LFECL. Therefore, the leakage flux eddy current first increases and then decreases with the length of air gap.

In addition, with the decrease in the permeability of nanocrystalline ribbons, R_{nano} increases and ϕ_3 increases. Thus, the leakage magnetic flux penetrating the internal ribbon increases, leading to the increases of leakage flux eddy current in the internal ribbons and the total LFECL. Therefore, the air gap and frequency-dependent permeability should be considered for the accurate estimation of LFECL

$$\begin{aligned} l_g \uparrow &\Rightarrow R_{\text{air}} \uparrow \Rightarrow \text{leakage flux in the } n\text{th ribbon first} \\ &\uparrow \text{and then} \downarrow \\ &\Rightarrow \text{loss first} \uparrow \text{and then} \downarrow \end{aligned} \tag{17}$$

$$\mu_{\text{nano}} \downarrow \Rightarrow R_{\text{nano}} \uparrow \Rightarrow \text{leakage flux in the } n\text{th ribbon} \uparrow \Rightarrow \text{loss} \uparrow. \tag{18}$$

For HFT with separated windings, taking several ribbons as illustrated in Fig. 21(a) as an example, an equivalent magnetic circuit is established as illustrated in Fig. 21(b). The reverse MMF sources, which model the reverse magnetic flux induced by the eddy currents in ribbon sections, are not connected in series with $R_{\text{nano},i}$ in Fig. 21(b). Instead, frequency-dependent permeability is adopted to account for the demagnetization effect of induced eddy currents in ribbon sections. Due to the symmetry of the transformer structure and magnetic circuit, the magnetic flux will not flow through the air gap. In Fig. 21(b), the flux through R_{air} is zero and the upper and lower parts of the magnetic circuit can be decoupled. When the length of the air gap increases from zero to nonzero, the leakage flux eddy current path is cut off and the LFECL decreases. When the primary current is constant, with the increase of air gap length, the magnetizing inductance of the transformer decreases and then the secondary current decreases. Thus, the leakage magnetic flux produced by the secondary winding decreases and the LFECL decreases. In addition, with the decrease of permeability of nanocrystalline ribbons, $R_{\text{nano},n}$ increases and ϕ_3 increases. Thus, the leakage

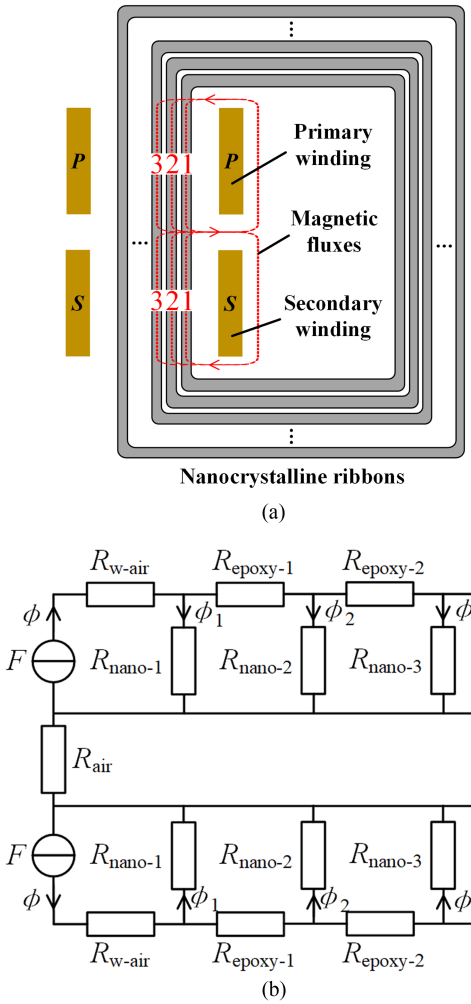

Fig. 21. Schematic diagram of leakage flux paths in the HFT with separated windings. (a) Example of leakage flux paths in the nanocrystalline core composed of several ribbons. (b) Equivalent magnetic circuit model.

magnetic flux penetrating the internal ribbon increases, leading to the increases of leakage flux eddy current in the internal ribbons and the total LFECL

$$l_g : \text{zero} \rightarrow \text{nonzero} \Rightarrow \text{leakage flux eddy current} \downarrow \Rightarrow \text{loss} \downarrow$$
$$l_g \uparrow \Rightarrow \text{magnetizing inductance} \downarrow \Rightarrow \text{secondary current} \downarrow \Rightarrow \text{loss} \downarrow \quad (19)$$
$$\mu_{\text{nano}} \downarrow \Rightarrow R_{\text{nano}} \uparrow \Rightarrow \text{leakage flux in the } n\text{th ribbon} \uparrow \Rightarrow \text{loss} \uparrow . \quad (20)$$

B. Simulation Results

The sensitivities of LFECLR R_{leakage} to the air gap length, permeability, and frequency are investigated by FE simulations. Fig. 22 shows the sensitivity of LFECLR for the HFT with concentric windings. As demonstrated in Fig. 22(a), from 0 to 1 mm, R_{leakage} increases with the length of the air gap. The reason is that with the increase of air gap length, the reluctance of air gap increases, and the magnetic flux penetrating the internal ribbons increases. From 1 to 5 mm, R_{leakage} decreases with the length of air gap. The reason is that when the length of air gap is large, the total reluctance of the magnetic path increases and the leakage flux decreases. Fig. 22(b) shows that R_{leakage} decreases with permeability since the magnetic flux penetrating the internal ribbons decreases with permeability. The impact

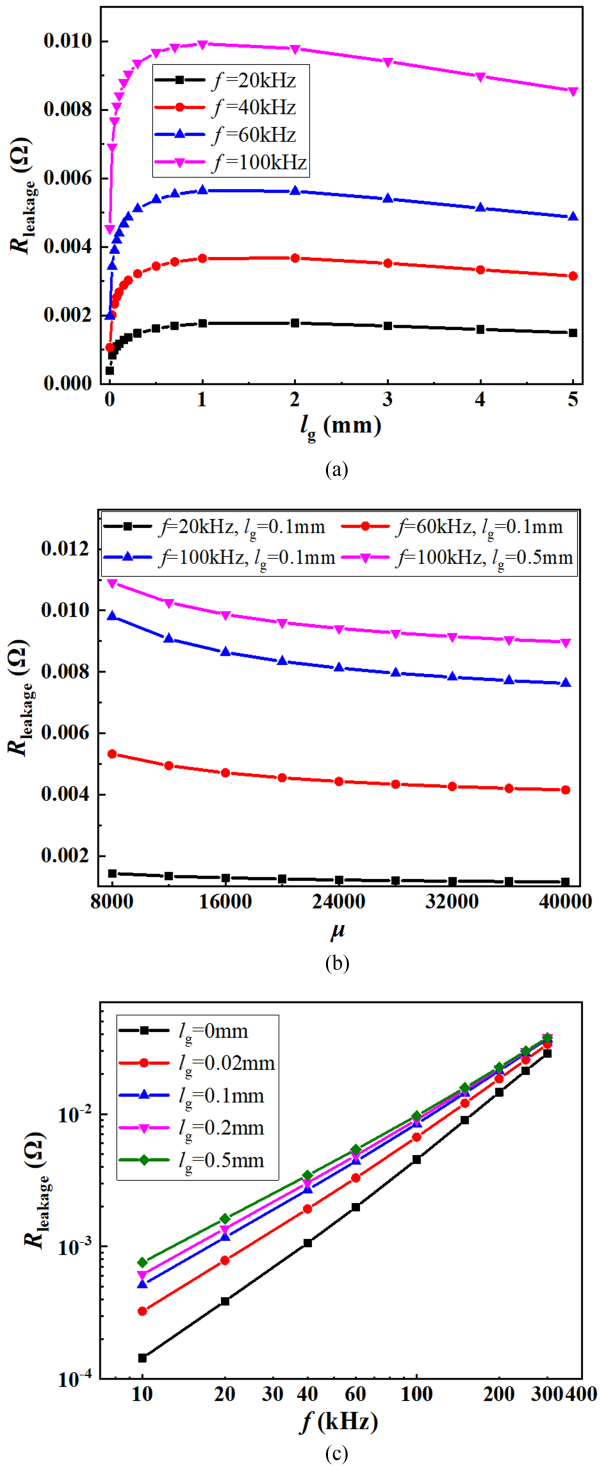

Fig. 22. Sensitivities of LFECLR R_{leakage} to (a) the length of air gap, (b) permeability of nanocrystalline ribbon, and (c) frequency for the transformer with concentric windings.

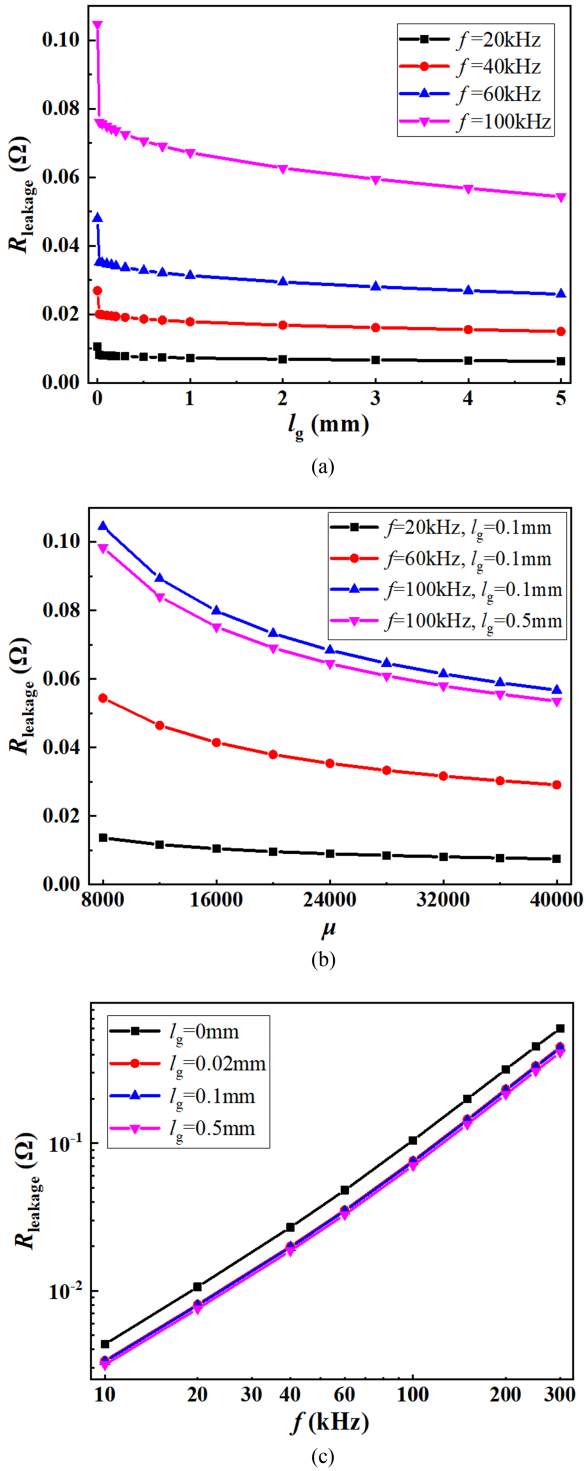

Fig. 23. Sensitivities of LFECLR R_{leakage} to (a) the length of air gap, (b) permeability of nanocrystalline ribbon, and (c) frequency for the transformer with separated windings.

of permeability on the LFECLR is not significant when the permeability is large. Fig. 22(c) shows that R_{leakage} increases exponentially with the frequency. In addition, the exponential coefficient decreases with the length of air gap.

Fig. 23 shows the sensitivities of LFECLR for the HFT with separated windings. As illustrated in Fig. 23(a), when the length of air gap increases from zero to nonzero, the LFECLR drops sharply since the eddy current near the air gap is cut OFF. With the increase in air gap length, the LFECLR decreases slightly. The reason is that the magnetizing inductance of the transformer decreases with frequency and the current and leakage magnetic flux in the secondary winding decreases. Fig. 23(b) shows that R_{leakage} decreases with permeability since the magnetic flux penetrating the internal ribbons decreases with permeability. The sensitivity of R_{leakage} to permeability for the HFT with separated windings is higher than the HFT with concentric windings. Fig. 23(c) shows that R_{leakage} increases exponentially with the frequency. In addition, the exponential coefficients are almost independent of the length of air gap.

VI. Conclusion

This article proposes a deduction measurement method and high-accuracy calculation model for the LFECLR in the nanocrystalline core. The main conclusions are listed as follows.

1) The LFECLR can be obtained by deduction of winding ac resistance and core loss resistance from total ac resistance. The winding ac resistance can be measured on a ferrite core HFT with identical core and winding sizes.
2) The air gap and permeability can change the leakage flux eddy current distribution in the nanocrystalline core. The proposed homogenization FE model considering air gap and frequency-dependent permeability can accurately calculate the LFECLR. The mean errors of the proposed model for the two HFT prototypes are reduced from 55.9% and 12.5% to 2.56% and 7.2%.
3) The LFECLR decreases with permeability and increases with frequency. For the HFT with concentric windings, LFECLR first increases sharply and then decreases slowly with air gap length. For the HFT with separated windings, LFECLR decreases slowly with air gap length. The LFECLR for the nongapped core is much higher than the gapped core.

This article only studied the calculation model of LFECLR under small-signal sinusoidal excitation and short-circuit condition. However, the practical operation condition of HFT is large-signal nonsinusoidal excitation and load condition. In the future, the calculation method of LFECLR under nonsinusoidal excitation and load condition will be investigated.

References

[1] M. Yilmaz and P. T. Krein, "Review of battery charger topologies, charging power levels, and infrastructure for plug-in electric and hybrid vehicles," *IEEE Trans. Power Electron.*, vol. 28, no. 5, pp. 2151–2169, May 2013.
[2] L. Zheng, R. P. Kandula, and D. Divan, "Multiport control with partial power processing in solid-state transformer for pv, storage, and fast-charging electric vehicle integration," *IEEE Trans. Power Electron.*, vol. 38, no. 2, pp. 2606–2616, Feb. 2023.
[3] C. Gu, Z. Zheng, L. Xu, K. Wang, and Y. Li, "Modeling and control of a multiport power electronic transformer (PET) for electric traction applications," *IEEE Trans. Power Electron.*, vol. 31, no. 2, pp. 915–927, Feb. 2016.
[4] J. Feng, W. Q. Chu, Z. Zhang, and Z. Q. Zhu, "Power electronic transformer-based railway traction systems: Challenges and opportunities," *IEEE J. Emerg. Sel. Topics Power Electron.*, vol. 5, no. 3, pp. 1237–1253, Sep. 2017.

[5] X. She, A. Q. Huang, and R. Burgos, "Review of solid-state transformer technologies and their application in power distribution systems," *IEEE J. Emerg. Sel. Topics Power Electron.*, vol. 1, no. 3, pp. 186–198, Sep. 2013.
[6] L. Zheng, R. P. Kandula, and D. Divan, "Current-source solid-state dc transformer integrating LVDC microgrid, energy storage, and renewable energy into MVDC grid," *IEEE Trans. Power Electron.*, vol. 37, no. 1, pp. 1044–1058, Jan. 2022.
[7] B. S. Ram, A. K. Paul, and S. V. Kulkarni, "Soft magnetic materials and their applications in transformers," *J. Mag. Mag. Mater.*, vol. 537, Nov. 2021, Art. no. 168210.
[8] C. P. Steinmetz, "On the law of hysteresis," *AIEE Trans.*, vol. 9, pp. 3–64, 1892.
[9] J. Reinert, A. Brockmeyer, and R. W. A. A. De Doncker, "Calculation of losses in ferro- and ferrimagnetic materials based on the modified Steinmetz equation," *IEEE Trans. Ind. Appl.*, vol. 37, no. 4, pp. 1055–1061, Jul./Aug. 2001.
[10] K. Venkatachalam, C. R. Sullivan, T. Abdallah, and H. Tacca, "Accurate prediction of ferrite core loss with nonsinusoidal waveforms using only Steinmetz parameters," in *Proc. IEEE Workshop Comput. Power Electron.*, 2002, pp. 36–41.
[11] W. Shen, F. Wang, D. Boroyevich, and C. W. Tipton, "Loss characterization and calculation of nanocrystalline cores for high-frequency magnetics applications," *IEEE Trans. Power Electron.*, vol. 23, no. 1, pp. 475–484, Jan. 2008.
[12] J. Muhlethaler, J. Biela, J. W. Kolar, and A. Ecklebe, "Improved core-loss calculation for magnetic components employed in power electronic systems," *IEEE Trans. Power Electron.*, vol. 27, no. 2, pp. 964–973, Feb. 2012.
[13] S. Barg, K. Ammous, H. Mejbri, and A. Ammous, "An improved empirical formulation for magnetic core losses estimation under nonsinusoidal induction," *IEEE Trans. Power Electron.*, vol. 32, no. 3, pp. 2146–2154, Mar. 2017.
[14] S. Yue, Y. Li, Q. Yang, X. Yu, and C. Zhang, "Comparative analysis of core loss calculation methods for magnetic materials under nonsinusoidal excitations," *IEEE Trans. Magn.*, vol. 54, no. 11, Nov. 2018, Art. no. 6300605.
[15] G. Bertotti, "General properties of power losses in soft ferromagnetic materials," *IEEE Trans. Magn.*, vol. 24, no. 1, pp. 621–630, Jan. 1988.
[16] A. Boglietti, A. Cavagnino, M. Lazzari, and M. Pastorelli, "Predicting iron losses in soft magnetic materials with arbitrary voltage supply: An engineering approach," *IEEE Trans. Magn.*, vol. 39, no. 2, pp. 981–989, Mar. 2003.
[17] W. A. Roshen, "A practical, accurate and very general core loss model for nonsinusoidal waveforms," *IEEE Trans. Power Electron.*, vol. 22, no. 1, pp. 30–40, Jan. 2007.
[18] D. M. Ionel, M. Popescu, S. J. Dellinger, T. J. E. Miller, R. J. Heideman, and M. I. McGilp, "On the variation with flux and frequency of the core loss coefficients in electrical machines," *IEEE Trans. Ind. Appl.*, vol. 42, no. 3, pp. 658–667, May/Jun. 2006.
[19] H. Zhao, H. H. Eldeeb, Y. Zhang, Y. Zhan, G. Xu, and O. A. Mohammed, "An improved core loss model of ferromagnetic materials considering high-frequency and nonsinusoidal supply," *IEEE Trans. Ind. Appl.*, vol. 57, no. 4, pp. 4336–4346, Jul./Aug. 2021.
[20] T. Wang and J. Yuan, "Improvement on loss separation method for core loss calculation under high-frequency sinusoidal and nonsinusoidal excitation," *IEEE Trans. Magn.*, vol. 58, no. 8, Aug. 2022, Art. no. 6301109.
[21] M. Leibl, G. Ortiz, and J. W. Kolar, "Design and experimental analysis of a medium-frequency transformer for solid-state transformer applications," *IEEE J. Emerg. Sel. Topics Power Electron.*, vol. 5, no. 1, pp. 110–123, Mar. 2017.
[22] B. Chen, X. Liang, and N. Wan, "Design methodology for inductor-integrated litz-wired high-power medium-frequency transformer with the nanocrystalline core material for isolated DC-link stage of solid-state transformer," *IEEE Trans. Power Electron.*, vol. 35, no. 11, pp. 11557–11573, Nov. 2020.
[23] Z. Guo, R. Yu, W. Xu, X. Feng, and A. Q. Huang, "Design and optimization of a 200-kW medium-frequency transformer for medium-voltage SiC PV inverters," *IEEE Trans. Power Electron.*, vol. 36, no. 9, pp. 10548–10560, Sep. 2021.
[24] H. Hamzehbahmani, P. Anderson, J. Hall, and D. Fox, "Eddy current loss estimation of edge burr-affected magnetic laminations based on equivalent electrical network—Part I: Fundamental concepts and FEM modeling," *IEEE Trans. Power Del.*, vol. 29, no. 2, pp. 642–650, Apr. 2014.
[25] H. Hamzehbahmani, P. Anderson, J. Hall, and D. Fox, "Eddy current loss estimation of edge burr-affected magnetic laminations based on equivalent electrical network—Part II: Analytical modeling and experimental results," *IEEE Trans. Power Del.*, vol. 29, no. 2, pp. 651–659, Apr. 2014.
[26] B. Cougo and J. W. Kolar, "Integration of leakage inductance in tape wound core transformers for dual active bridge converters," in *Proc. 7th Int. Conf. Integr. Power Electron. Syst.*, Mar. 2012, pp. 1–6.
[27] R. B. Beddingfield, A. M. Leary, R. Noebe, M. Nations, R. Bowman, and S. Bhattacharya, "Calculation of transformer leakage inductance by simplified flux path geometries," in *Proc. IEEE Energy Convers. Congr. Expo.*, Oct. 2022, pp. 1–8.
[28] C. Chen, Z. Guo, R. Yu, and A. Q. Huang, "A novel hybrid core structure for 100kW medium frequency transformers," in *Proc. IEEE Energy Convers. Congr. Expo.*, Oct. 2023, pp. 5651–5657.
[29] B. X. Foo, A. L. F. Stein, and C. R. Sullivan, "A step-by-step guide to extracting winding resistance from an impedance measurement," in *Proc. IEEE Appl. Power Electron. Conf. Expo.*, 2017, pp. 861–867.
[30] X. Liu, L. Zhao, C. Ma, Q. Ge, and Y. Li, "Optimization simulation analysis of leakage magnetic field and loss characteristics of high frequency nanocrystalline transformer," in *Proc. 25th Int. Conf. Elect. Mach. Syst.*, Nov. 2022, pp. 1–6.
[31] Y. Liu, X. Liu, Z. Yin, K. Dong, C. Ma, and D. Cui, "Research on leakage inductance and eddy current loss of nanocrystalline high-frequency transformers," in *Proc. 26th Int. Conf. Elect. Mach. Syst.*, Dec. 2023, pp. 4560–4564.
[32] Z. Gao, H. Li, and F. Wang, "A medium-voltage transformer with integrated leakage inductance for 10 kV SiC-based dual-active-bridge converter," in *Proc. IEEE 9th Workshop Wide Bandgap Power Devices Appl.*, Nov. 2022, pp. 221–226.
[33] Z. Gao, D. Li, R. Chen, H. Bai, L. Tolbert, and F. Wang, "Design of A 50-kW medium frequency medium voltage transformer for 10-kV SiC-based dual active bridge converter," in *Proc. IEEE Energy Convers. Congr. Expo.*, Oct. 2023, pp. 5839–5845.
[34] J. Wang, H. Lin, Y. Huang, and X. Sun, "A new formulation of anisotropic equivalent conductivity in laminations," *IEEE Trans. Magn.*, vol. 47, no. 5, pp. 1378–1381, May 2011.
[35] S. Odawara et al., "Iron loss evaluation of reactor core with air gaps by magnetic field analysis under high-frequency excitation," *IEEE Trans. Magn.*, vol. 51, no. 11, Nov. 2015, Art. no. 8402404.
[36] Y. Wang, G. Calderon-Lopez, and A. J. Forsyth, "High-frequency gap losses in nanocrystalline cores," *IEEE Trans. Power Electron.*, vol. 32, no. 6, pp. 4683–4690, Jun. 2017.
[37] G. Calderon-Lopez, Y. Wang, and A. J. Forsyth, "Mitigation of gap losses in nanocrystalline tape-wound cores," *IEEE Trans. Power Electron.*, vol. 34, no. 5, pp. 4656–4664, May 2019.
[38] J. Liu, Q. Deng, D. Czarkowski, M. K. Kazimierczuk, H. Zhou, and W. Hu, "Frequency optimization for inductive power transfer based on ac resistance evaluation in litz-wire coil," *IEEE Trans. Power Electron.*, vol. 34, no. 3, pp. 2355–2363, Mar. 2019.
[39] K. Venkatachalam, C. R. Sullivan, T. Abdallah, and H. Tacca, "Accurate prediction of ferrite core loss with nonsinusoidal waveforms using only Steinmetz parameters," in *Proc. IEEE Workshop Comput. Power Electron.*, 2002, pp. 36–41.

Zhanlei Liu (Student Member, IEEE) was born in Hebei, China, in 1998. He received the B.S. degree in electrical engineering from Xi'an Jiaotong University, Xi'an, China, in 2020. He is currently working toward the Ph.D. degree in electrical engineering with Xi'an Jiaotong University, Xi'an, China.

His research interests include modeling of high-frequency magnetic materials and thermal design of high-frequency transformers.

Lingyu Zhu (Senior Member, IEEE) was born in Shandong, China, in 1988. He received the B.Sc. and Ph.D. degrees in electrical engineering from Xi'an Jiaotong University, Xi'an, China, in 2009 and 2014, respectively.

He is currently a full Professor with Xi'an Jiaotong University. His research interest focuses on condition monitoring of power equipment in HVdc application.

Yongliang Dang was born in Gansu, China, in 1996. He received the B.S. degree in electrical engineering in 2018 from Xi'an Jiaotong University, Xi'an, China, where he is currently working toward the Ph.D. degree in electrical engineering.

His research interests include modeling of high-frequency magnetic component in power electronic equipment.

Cao Zhan (Member, IEEE) received the B.S. and Ph.D. degrees in electrical engineering from Xi'an Jiaotong University, Xi'an, China, in 2015 and 2022, respectively.

From October 2016 to September 2017, he was a visiting student with RWTH Aachen University, Aachen, Germany. From 2023 to 2023, he was an Assistant Professor with the Department of Electrical Engineering, Xi'an Jiaotong University. He is currently a Postdoc Associate with the Bradley Department of Electrical and Computer Engineering (ECE), Virginia Tech, Blacksburg, VA, USA, working in the Center for Power Electronics Systems (CPES). His research interests include power electronics packaging and integration for wide-bandgap and ultra-wide-bandgap power semiconductor devices; electrical, thermal, and reliability characterization and test of power semiconductor devices; intelligent monitoring and diagnosis of power electronic and high voltage equipment.

Shengchang Ji (Member, IEEE) was born in Shandong, China, in 1976. He received the B.Sc. and Ph.D. degrees in electrical engineering from Xi'an Jiaotong University, Xi'an, China, in 1998 and 2003, respectively.

He is currently a Professor with Xi'an Jiaotong University, Xi'an, China. His research interest focuses on condition monitoring of power equipment in HVdc application.